

Structure and motifs of iron oxides from 1 to 3 TPa

Feng Zheng,¹ Yang Sun,^{2,*} Renhai Wang,^{3,4} Yimei Fang,¹ Feng Zhang,⁴ Shunqing Wu,^{1,†} Cai-Zhuang Wang,⁴ Renata M. Wentzcovitch,^{2,5,6,‡} and Kai-Ming Ho⁴

¹*Department of Physics, OSED,
Key Laboratory of Low Dimensional Condensed Matter Physics
(Department of Education of Fujian Province)*

Jiujiang Research institute, Xiamen University, Xiamen 361005, China.

²*Department of Applied Physics and Applied Mathematics,
Columbia University, New York, NY, 10027, USA*

³*School of Physics and Optoelectronic Engineering,
Guangdong University of Technology, Guangzhou 510006, China*

⁴*Department of Physics, Iowa State University, Ames, Iowa 50011, United States*

⁵*Department of Earth and Environmental Sciences,
Columbia University, New York, NY, 10027, USA*

⁶*Lamont-Doherty Earth Observatory, Columbia University, Palisades, NY, 10964, USA*

(Dated: Oct. 28, 2021)

Iron oxides are fundamental components of planet-forming materials. Understanding the Fe-O system's behavior and properties under high pressure can help us identify many new phases and states possible in exoplanetary interiors, especially terrestrial ones. Using the adaptive genetic algorithm (AGA), we investigate the structure of iron oxides for a wide range of stoichiometries ($0.25 \leq x_O \leq 0.8$) at 1, 2, and 3 TPa. Five unreported ground-state structures with Fe_2O , FeO , Fe_3O_5 , FeO_2 , and FeO_4 compositions are identified. The calculated density of states (DOS) suggests that, except for FeO_4 , all phases are metallic, but their carrier densities decrease with increasing pressure and oxygen content. The cluster alignment analysis of stable and metastable phases shows that several motifs may co-exist in a structure of iron oxides with low O content. In contrast, most iron oxides with high O content adopt a simple BCC motif at TPa pressures. Our results provide a crystal structure database of iron oxides for modeling and understanding the interiors of exoplanets.

I. INTRODUCTION

Iron and oxygen are the two most significant elements of Earth-like exoplanets [1]. Studies on iron oxides' structures and fundamental properties provide a valuable understanding of exoplanet forming phases, particularly terrestrial ones. Their high-pressure behavior has received considerable attention to advance understanding of Earth's interior. So far, at ambient or low pressures, three basic iron oxides have been known, i.e., wüstite FeO [2] magnetite Fe_3O_4 [3, 4], and hematite Fe_2O_3 [5, 6]. Previous studies revealed that these three iron oxides undergo complex electronic [7], magnetic [7, 8], and structural transformations [8–10] at high pressure, which can not only lead to seismic anomalies but also affect geochemical processes in Earth's interior. Besides the three basic iron oxides, several new stoichiometries of compounds were also synthesized at high pressure, such as Fe_4O_5 [11], Fe_5O_6 [12], Fe_5O_7 [10] and Fe_7O_9 [13], suggesting a complex phase diagram of iron oxides. Recently, using ab initio random structure searching (AIRSS), Weerasinghe *et al.* identified a series of stable and metastable Fe-O compounds at 100, 350, and 500 GPa [14], which further broadens the database

of the Fe-O system at high pressure. It is worth noting that the predicted pyrite-type FeO_2 was later confirmed by experimental synthesis [15]. This successful discovery is impactful and demonstrates that computational predictions can play a significant role in discovering high-pressure phases.

However, up to now, most attention has been focused on elucidating the nature of structures and phase transitions of iron oxides below 500 GPa. A legitimate question is: what are the subsequent high-pressure phases of iron oxides? The answer can provide insights into the types of coordination preferred by iron in planet-forming silicates and oxides and possible, stable phases in solid parts of terrestrial planetary cores where pressures can reach ~ 4 TPa [16]. These exoplanets frequently referred to as "super-Earths" [17], have a similar interior structure and composition with Earth, which is dominated by the elements Fe and O [1, 17]. Modeling and understanding these planetary interiors can help us investigate their potential habitability, but it requires a basic knowledge of planet-forming phases and their properties under extreme conditions. In this paper, using an adaptive genetic algorithm (AGA) [18], we study the Fe-O compounds at 1, 2, and 3 TPa across a wide range of stoichiometries ($0.25 \leq x_O \leq 0.8$). The local packing motifs in the stable and metastable Fe-O compounds are analyzed as a function of O contents.

* ys3339@columbia.edu

† wsq@xmu.edu.cn

‡ rmw2150@columbia.edu

II. COMPUTATIONAL METHODS

In this work, Fe-O's crystal structures were determined using the AGA method [18], which combines fast structure exploration by auxiliary classical potentials and the accurate ab initio calculations adaptively and iteratively. The Fe and O atoms' initial atomic positions were randomly generated in the GA-loop without assuming the Bravais lattice type, symmetry, atom basis, or unit cell dimensions. The total structure pool in our GA search was set to be 128. Structure searches with auxiliary interatomic potentials were performed 500 consecutive GA generations. Then, the 16 lowest-enthalpy structures at the end of each GA search were selected for single point DFT calculations according to the AGA procedure [18], whose energies, force, and stress are used to adjust the interatomic potential parameters for the next iteration of GA search. A total of 40 adaptive iterations were performed to obtain the final structures.

Here, the embedded-atom method (EAM) [19] was used as classical auxiliary potential. In EAM, the total energy of an N-atom system was evaluated by

$$E_{total} = \frac{1}{2} \sum_{i,j(i \neq j)}^N \varphi(r_{ij}) + \sum_i F_i(n_i) \quad (1)$$

where $\varphi(r_{ij})$ denotes the pair repulsion between atoms i and j with a distance of r_{ij} , $F_i(n_i)$ is the embedded term with electron density term $n_i = \sum_{j \neq i} \rho_j(r_{ij})$ at the site occupied by atom i . The fitting parameters in the EAM formula were chosen as follows: The parameters for Fe-Fe interactions were taken from the literature [20], while the Fe-O and O-O interactions were modeled by Morse function,

$$\varphi(r_{ij}) = D[e^{-2\alpha(r_{ij}-r_0)} - 2e^{-\alpha(r_{ij}-r_0)}], \quad (2)$$

where D , α and r_0 are the fitting parameters. The density function for O atoms is modeled by an exponentially decaying function

$$\rho(r_{ij}) = \alpha \exp[-\beta(r_{ij} - r_0)], \quad (3)$$

α and β are fitting parameters. The form proposed by Benerjea and Smith in Ref. [21] was used as the embedding function with fitting parameters F_0, γ as,

$$F(n) = F_0[1 - \gamma \ln n]n^\gamma. \quad (4)$$

For Fe, the density function and embedding function parameters were taken from Ref. [20]. The potential fitting was performed by the force-matching method with a stochastic simulated annealing algorithm as implemented in the POTFIT code [22, 23].

First-principles calculations were carried out using the Quantum ESPRESSO (QE) code [24, 25]. Our calculations suggest that magnetic order is destroyed at ultra-high pressures. The spin polarized state in all these compounds at 1 TPa and higher pressures is unstable. For

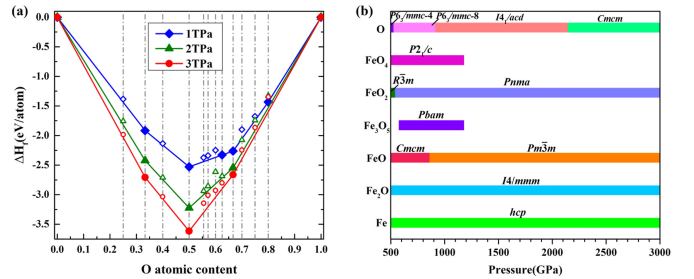


FIG. 1. (a) Convex hull diagrams of the Fe-O system at 1, 2, and 3 TPa. (b) Pressure stability fields of stable phases in the Fe-O system.

this reason, the non-spin-polarized generalized-gradient approximation (GGA) parameterized by Perdew-Burke-Ernzerhof formula (PBE) was used to describe the exchange-correlation energy. A kinetic-energy cutoff of 50 Ry for wave functions and 500 Ry for potentials were used. Brillouin-zone integration was performed over a k -point grid of $2\pi \times 0.03 \text{ \AA}^{-1}$ in the structure refinement. The convergence thresholds are 0.01 eV/ \AA for the atomic force, 0.5 kbar for the pressure, and 1×10^{-5} eV for the total energy. The structural optimization was performed under constant using the Broydon-Fletcher Goldfarb-Shanno (BFGS) algorithm [26–30] with variable cell shape. Phonon dispersions were calculated using the finite displacement method as implemented in the PHONOPY software [31, 32].

III. RESULTS AND DISCUSSION

A. AGA search for the Fe-O system

In order to obtain low-enthalpy structures of iron oxides, a wide range of stoichiometries of Fe_xO_y ($x : y = 3:1, 2:1, 3:2, 1:1, 4:5, 3:4, 2:3, 3:5, 1:2, 3:7, 1:3, 1:4$) with different formula units (i.e., 1, 2, 3, 4, 5, 6 and 8 f.u.) containing up to 40 atoms are searched at 1, 2 and 3 TPa, respectively. The relative stability of these predicted Fe-O compounds was investigated under the corresponding pressure, depending on the calculated formation enthalpies,

$$H_f = \frac{H_{\text{Fe}_x\text{O}_y} - xH_{\text{Fe}} - yH_{\text{O}}}{x + y}, \quad (5)$$

where H is the calculated enthalpy for a given structure, x and y are the numbers of atoms of Fe and O, respectively. Before we discuss the stable structures of iron oxides, the crystal structures of pure Fe and O should be clarified. For elemental Fe, our calculated results suggest that the Fe-hcp with $P6_3/mmc$ symmetry is the ground state phase from 1 to 3 TPa. While for oxygen, the $I4_1/acd$ structure is predicted to be stable at 1 and 2

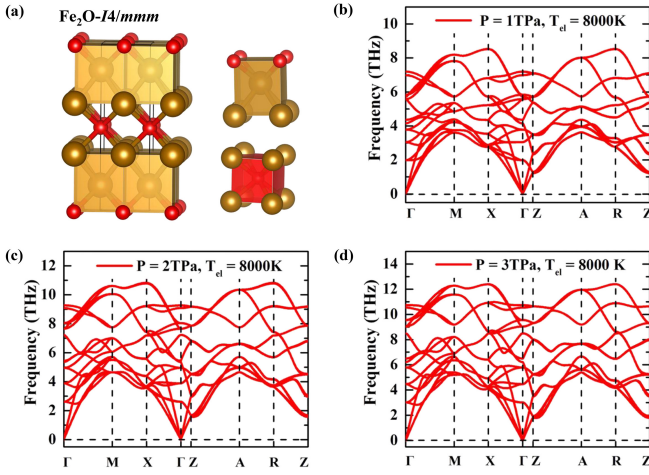


FIG. 2. (a) Crystal structure and Fe and O coordination polyhedra of $I4/mmm$ Fe_2O . Fe and O atoms are denoted by light brown and red spheres, respectively; Phonon dispersions of $I4/mmm$ Fe_2O with $T_{el} = 8000\text{ K}$ at (b) 1TPa, (c) 2TPa, and (d) 3TPa.

TPa. At 3 TPa, oxygen adopts a structure with $Cmcm$ symmetry. The stable structures of Fe and oxygen are shown in Fig. S1. Fig. 1(a) presents convex hulls of the Fe-O system at 1, 2, and 3 TPa. Five Fe_xO_y stoichiometries are found in these hulls, i.e., Fe_2O , FeO , Fe_3O_5 , FeO_2 and FeO_4 . As shown in Fig. 1(b), the stability fields of these phases were investigated from 500 GPa to the upper limit for the pressure considered in Ref. [14], to 3 TPa. For Fe_2O , Weerasinghe et al. predicted that an $I4/mmm$ phase could be stable from 288 GPa to 500 GPa [14]. Here, we show that it can withstand high pressures up to 3 TPa. Previous DFT calculations show that FeO undergoes a complex structural transformation in the pressure range of the Earth's interior [14, 33]. At ultrahigh pressures, our results suggest that the phase with $Cmcm$ symmetry is the ground-state from 500 to 860 GPa. At 860 GPa, the $Cmcm$ phase is predicted to transform into a phase of $Pm\bar{3}m$ symmetry (CsCl-type structure), which remains stable up to 3 TPa. Above 575 GPa, the Fe_3O_5 phase is stable in an orthorhombic structure with the $Pbam$ symmetry. While, at pressures above 1180 GPa, this phase decomposes into FeO and FeO_2 . For FeO_2 , Weerasinghe et al. identified the FeO_2 phase with $Pa\bar{3}$ symmetry [14], which is stable from 100 to 456 GPa. This pyrite-type FeO_2 phase has recently been confirmed by experiments [15]. At 456 GPa, the $Pa\bar{3}$ phase is predicted to transform to a phase with $R\bar{3}m$ symmetry [14]. Here, we show that $R\bar{3}m$ FeO_2 should transform to a new phase with $Pnma$ symmetry at 540 GPa, and $Pnma$ FeO_2 can be stable to at least 3 TPa. At 500 GPa, FeO_4 adopts a structure with $P2_1/c$ symmetry. At 1180 GPa, $P2_1/c$ FeO_4 decomposes into FeO_2 and O. The structural parameters of these stable iron oxides are listed in Supplementary Table S1.

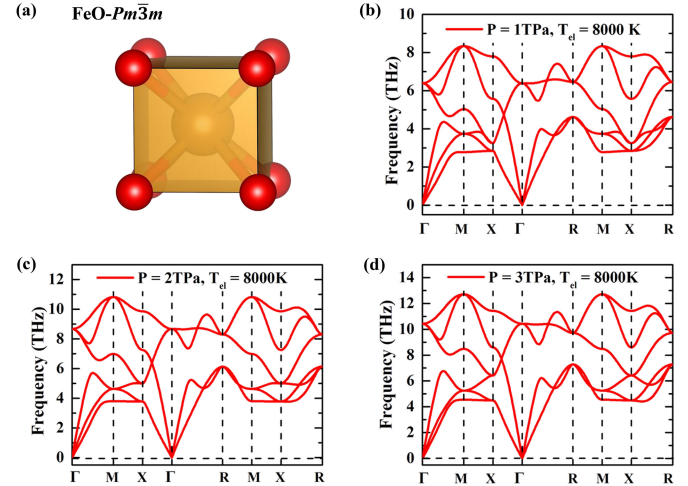


FIG. 3. (a) Crystal structure of $Pm\bar{3}m$ FeO . Fe and O atoms are denoted by light brown and red spheres, respectively. Phonon dispersions of $Pm\bar{3}m$ FeO with $T_{el} = 8000\text{ K}$ at (b) 1TPa, (c) 2TPa and (d) 3TPa.

B. Crystal structure for stable Fe-O compounds

Fe₂O. Fig. 2 shows the crystal structure and phonon dispersion for tetragonal Fe_2O with $I4/mmm$ symmetry. In this structure, each Fe is coordinated to four Fe's and four O's, while each O is coordinated to eight Fe's. These motifs pack in the face-sharing arrangement. This structure is the same as the $I4/mmm$ -type phases of Fe_2Mg [34] and Al_2S [35]. The calculated phonon spectrum confirms that this phase is dynamically stable at 1, 2 and 3 TPa with an electron temperature (T_{el}) of 8000 K as seen in Fig. 2 (b)-(d). Because the temperature at the core-mantle boundary of a super-Earth falls within the range from 4000K to 10000 K [16], the choice of $T_{el} = 8000\text{ K}$ is reasonable. Nevertheless, phonon dispersions with $T_{el} = 150\text{ K}$ are also presented in Fig. S2, showing no imaginary frequencies in the entire Brillouin zone.

FeO. The phase with $Cmcm$ symmetry is the ground state structure of FeO from 500 to 860 GPa (Fig. S1(d)). From 860 GPa to 3 TPa, FeO stabilizes in the CsCl-type (B2) structure with $Pm\bar{3}m$ symmetry as shown in Fig. 3(a). Phonon calculations confirm its dynamic stability at 1, 2 and 3 TPa with $T_{el} = 8000\text{ K}$ (Fig. 3(b)-(d)). At low electron temperature ($T_{el} = 150\text{ K}$), our calculated results show that it is also dynamically stable, as seen in Fig. S3.

Fe₃O₅. From 575 GPa to 1180 GPa, Fe_3O_5 adopts an orthorhombic phase with $Pbam$ space group (see Fig. 1(b)). In this structure, each Fe is 8-fold coordinated by O's and form face-shared and edge/face diagonal-shared (an edge in one cube shares with a face diagonal of another cube) cubes, as seen in Fig. 4(a). The calculated phonon dispersion shows the $Pbam$ Fe_3O_5 is dynamically stable at 1TPa with $T_{el} = 8000\text{ K}$ (Fig. 4(b)) and $T_{el} =$

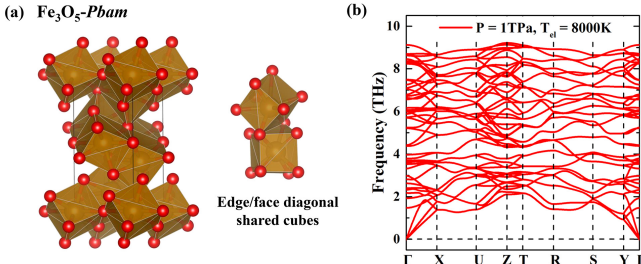


FIG. 4. (a) Crystal structure and edge/face diagonal shared cubes of $Pnam$ Fe_3O_5 . Light brown and red spheres denote Fe and O, respectively; (b) Phonon dispersion of $Pnam$ Fe_3O_5 at 1 TPa with $T_{el} = 8000$ K.

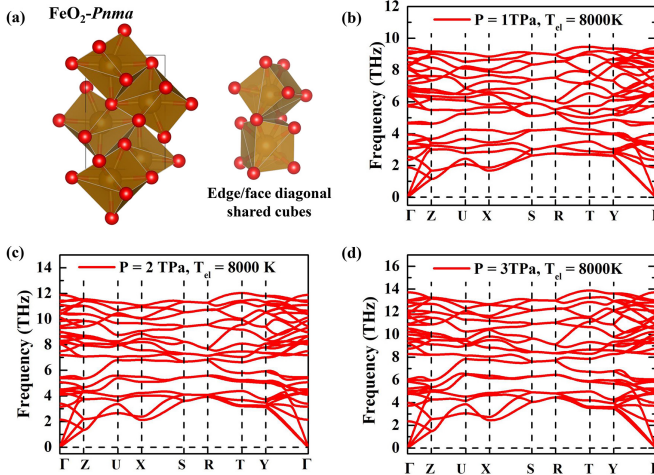


FIG. 5. (a) Crystal structure and edge/face diagonal shared cubes of $Pnma$ FeO_2 . Light brown and red spheres denote Fe and O, respectively. Phonon dispersions of $Pnam$ FeO_2 at (b) 1 TPa, (c) 2TPa and (d) 3TPa with $T_{el} = 8000$ K.

150 K (Fig. S4). At 1180 GPa, this structure decomposes into FeO and FeO_2 .

FeO₂. The ground-state structure of FeO_2 is orthorhombic with $Pnma$ symmetry from 540 GPa to 3 TPa, as seen in Fig. 5(a). In this structure, each Fe is coordinated by 8 O's forming distorted FeO_8 cubes. These cubes pack in a similar arrangement to that in $Pbam$ Fe_3O_5 . The dynamic stability of the $Pnam$ FeO_2 is verified by the absence of imaginary frequencies in the phonon dispersion at 1, 2 and 3 TPa with $T_{el} = 8000$ K as shown in Fig. 5(b)-(d). Phonon dispersions with $T_{el} = 150$ K are shown in Fig. S5.

FeO₄. Fig. 6 plots the crystal structure and phonon dispersion for the FeO_4 with $P2_1/c$ symmetry. Each Fe is coordinated with 8 O's to form edge-shared cubes. The calculated phonon dispersion shows this $P2_1/c$ FeO_4 phase is dynamically stable at 1 TPa with $T_{el} = 8000$ K (Fig. 6(b)) and $T_{el} = 150$ K (Fig. S6).

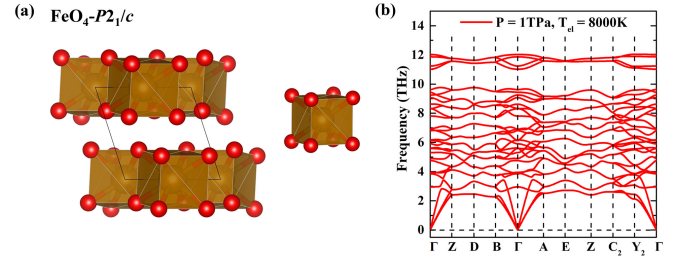


FIG. 6. (a) Crystal structure of $P2_1/c$ FeO_4 . Light brown and red spheres denote Fe and O, respectively; (b) Phonon dispersion of $P2_1/c$ FeO_4 at 1TPa with $T_{el} = 8000$ K.

The electronic density of states (DOS) at the Fermi level (EF) of these five Fe-O compounds is investigated from 1 to 3 TPa. As shown in Fig. 7, our calculations indicate that, except for FeO_4 , all iron oxides phases identified are metallic. Whether or not this is an artifact of the gap underestimation by PBE/GGA should be investigated in the future. As expected, for a given Fe_xO_y stoichiometry, results indicate that the carrier density decreases with increasing pressure. FeO_4 remains an insulating phase up to 3 TPa, despite the PBE/GGA gap underestimation. The calculated DOS of these five iron oxides at 1, 2 and 3 TPa are shown in Fig. S7-S11.

C. Analysis of structure motifs of Fe-O system under pressure

Besides the stable Fe-O compounds, we also predicted several metastable structures in the Fe-O system from 1 to 3TPa. Since the current calculation does not consider temperature effects on structural stability, these low enthalpy metastable iron oxides may become stable at finite temperatures. Therefore, it is necessary to investigate structural motifs of these stable and metastable Fe_xO_y phases to reveal overall structural features in the Fe-O system at high pressures. Here, the threshold for metastability is set to their relative enthalpies (H_d) w.r.t the convex hull by 0.3 eV/atom. The Fe-centered clusters in these iron oxides were defined by using the cluster alignment method [36]. Four typical motifs, including BCC, BCT (body-centered tetragonal), FCC, and HCP are used as templates. We also include the "161" motif (two face-shared hexagonal caps), which is a common cluster in Fe-O binary compounds at high pressure [14].

Snapshots of these motifs are shown in Fig. 8(a). We define an "alignment score" to quantify the similarity between aligned clusters and template motifs [36]. Here, the cutoff value of the alignment score is set to 0.125. If the alignment score is higher than 0.125, the cluster is marked as 'others', meaning the group of atoms cannot be classified into the current templates or is much more distorted than these perfect motifs.

Fig. 8(b)-(d) shows the relative enthalpies w.r.t. the

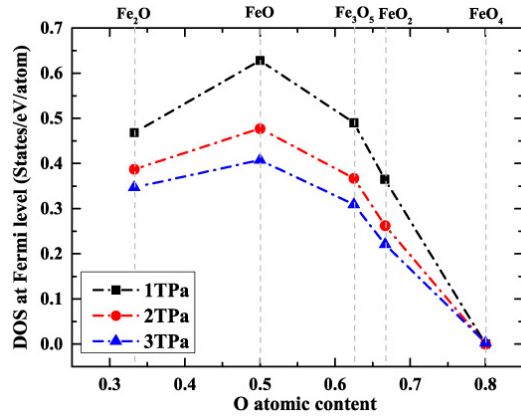


FIG. 7. (a) Pressure variation of the carrier density in Fe-O compounds.

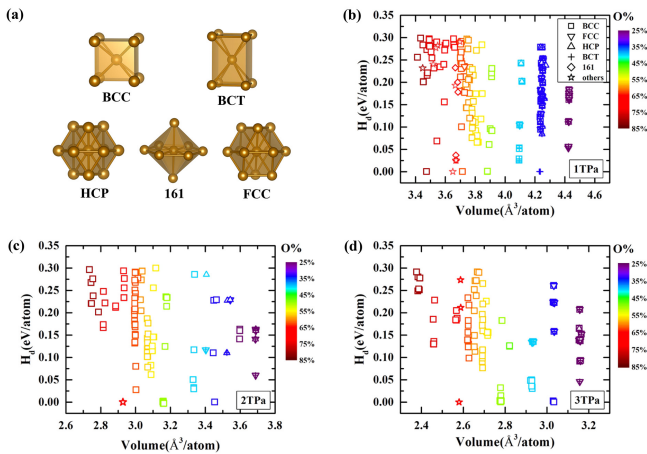


FIG. 8. (a) Five template motifs are considered here. Enthalpies above the convex-hull (H_d) of low-enthalpy Fe_xO_y structures as a function of their volumes at (b) 1TPa, (c) 2TPa, and (d) 3TPa, where the symbols denote the local packing motifs, and colors represent oxygen concentration.

convex hull of these stable and metastable iron oxides vs. their volumes. The types of Fe-centered clusters and

O concentrations are denoted with different symbols and colors, respectively. It can be found that, at 1, 2, and 3 TPa, several motifs may co-exist in Fe-O compound structures with low O content, while, for iron oxides with higher O content, most of them adopt simple BCC motifs, as seen in Fig. 8(b)-(d). Furthermore, we note that several motifs in iron oxides are determined as 'others' at 1, 2, and 3 TPa. Some of them may form more complex clusters than the considered templates, some just highly distorted template-like clusters, e.g., the ground-state *Pnma* FeO_2 structure (Fig. 5(a)).

IV. CONCLUSION

In summary, we use the AGA method to study structure in the Fe-O system across a wide range of stoichiometries at 1, 2, and 3 TPa. Several stable phases with stoichiometries Fe_2O , FeO , Fe_3O_5 , FeO_2 , and FeO_4 are identified. Except for FeO_4 , the calculated electronic density of states show these Fe-O compounds are metallic. As expected, the carrier density decreases with the increasing pressure. The cluster alignment analysis reveals that most low-enthalpy phases prefer a BCC packing motif at high pressure, especially those with high O content. This study provides the structural database for the Fe-O system, a preliminary step for understanding Fe and O bearing phases which are necessary for modeling planetary interiors.

ACKNOWLEDGMENTS

Work at Xiamen University was supported by the National Natural Science Foundation of China (11874307). Work at Iowa State University and Columbia University was supported by the National Science Foundation awards EAR-1918134 and EAR-1918126. Work at Guangdong University of Technology was supported by the Guangdong Natural Science Foundation of China (Grant No. 2017B030306003, and No.2019B1515120078). R.Wang also thank Center of Campus Network & Modern Educational Technology of GDUT for providing computational resources and technical support for this work.

-
- [1] A. E. Doyle, E. D. Young, B. Klein, B. Zuckerman, and H. E. Schlichting, *Science* **366**, 356–359 (2019).
 - [2] Y. Fei and H.-k. Mao, *Science* **266**, 1678–1680 (1994).
 - [3] M. P. Pasternak, S. Nasu, K. Wada, and S. Endo, *Phys. Rev. B* **50**, 6446 (1994).
 - [4] Y. Fei, D. J. Frost, H.-K. Mao, C. T. Prewitt, and D. Haeusermann, *Am. Mineral.* **84**, 203–206 (1999).
 - [5] G. K. Rozenberg, L. Dubrovinsky, M. Pasternak, O. Naaman, T. Le Bihan, and R. Ahuja, *Phys. Rev. B* **65**, 064112 (2002).
 - [6] J. Badro, G. Fiquet, V. V. Struzhkin, M. Somayazulu, H.-k. Mao, G. Shen, and T. Le Bihan, *Phys. Rev. Lett.* **89**, 205504 (2002).
 - [7] S.-H. Shim, A. Bengtson, D. Morgan, W. Sturhahn, K. Catalli, J. Zhao, M. Lerche, and V. Prakapenka, *Proc. Natl. Acad. Sci. U.S.A.* **106**, 5508–5512 (2009).
 - [8] S. Ju, T.-Y. Cai, H.-S. Lu, and C.-D. Gong, *J. Am. Chem. Soc.* **134**, 13780–13786 (2012).
 - [9] H. Ozawa, F. Takahashi, K. Hirose, Y. Ohishi, and N. Hirao, *Science* **334**, 792–794 (2011).

- [10] E. Bykova, L. Dubrovinsky, N. Dubrovinskaia, M. Bykov, C. McCammon, S. V. Ovsyannikov, H.-P. Liermann, I. Kupenko, A. I. Chumakov, R. Rüffer, et al., *Nat. Commun.* **7**, 1–6 (2016).
- [11] B. Lavina, P. Dera, E. Kim, Y. Meng, R. T. Downs, P. F. Weck, S. R. Sutton, and Y. Zhao, *Proc. Natl. Acad. Sci. U.S.A.* **108**, 17281–17285 (2011).
- [12] B. Lavina and Y. Meng, *Sci. Adv.* **1**, e1400260 (2015).
- [13] R. Sinmyo, E. Bykova, S. V. Ovsyannikov, C. McCammon, I. Kupenko, L. Ismailova, and L. Dubrovinsky, *Sci. Rep.* **6**, 1–7 (2016).
- [14] G. L. Weerasinghe, C. J. Pickard, and R. Needs, *J. Phys.: Condens. Matter* **27**, 455501 (2015).
- [15] Q. Hu, D. Y. Kim, W. Yang, L. Yang, Y. Meng, L. Zhang, and H.-K. Mao, *Nature* **534**, 241–244 (2016).
- [16] A. P. Van Den Berg, D. A. Yuen, K. Umemoto, M. H. Jacobs, and R. Wentzcovitch, *Icarus* **317**, 412–426 (2019).
- [17] S. Seager, M. Kuchner, C. Hier-Majumder, and B. Militzer, *Astrophys. J.* **669**, 1279 (2007).
- [18] S. Wu, M. Ji, C.-Z. Wang, M. C. Nguyen, X. Zhao, K. Umemoto, R. Wentzcovitch, and K.-M. Ho, *J. Phys.: Condens. Matter* **26**, 035402 (2013).
- [19] S. Foiles, M. Baskes, and M. S. Daw, *Phys. Rev. B* **33**, 7983 (1986).
- [20] X. Zhou, R. Johnson, and H. Wadley, *Phys. Rev. B* **69**, 144113 (2004).
- [21] A. Banerjea and J. R. Smith, *Phys. Rev. B* **37**, 6632 (1988).
- [22] P. Brommer and F. Gähler, *Philos. Mag.* **86**, 753–758 (2006).
- [23] P. Brommer and F. Gähler, *Modell. Simul. Mater. Sci. Eng.* **15**, 295 (2007).
- [24] P. Giannozzi, S. Baroni, N. Bonini, M. Calandra, R. Car, C. Cavazzoni, D. Ceresoli, G. L. Chiarotti, M. Cococcioni, I. Dabo, et al., *J. Phys.: Condens. Matter* **21**, 395502 (2009).
- [25] P. Giannozzi, O. Andreussi, T. Brumme, O. Bunau, M. B. Nardelli, M. Calandra, R. Car, C. Cavazzoni, D. Ceresoli, M. Cococcioni, et al., *J. Phys.: Condens. Matter* **29**, 465901 (2017).
- [26] C. G. Broyden, *IMA J. Appl. Math.* **6**, 76–90 (1970).
- [27] C. G. Broyden, *IMA J. Appl. Math.* **6**, 222–231 (1970).
- [28] R. Fletcher, *Comput. J.* **13**, 317–322 (1970).
- [29] D. Goldfarb, *Math. Comput.* **24**, 23–26 (1970).
- [30] D. F. Shanno, *Math. Comput.* **24**, 647–656 (1970).
- [31] A. Togo, F. Oba, and I. Tanaka, *Phys. Rev. B* **78**, 134106 (2008).
- [32] A. Togo and I. Tanaka, *Scr. Mater.* **108**, 1–5 (2015).
- [33] Y. Sun, M. Cococcioni, and R. M. Wentzcovitch, *Phys. Rev. Mater.* **4**, 063605 (2020).
- [34] P. Gao, C. Su, S. Shao, S. Wang, P. Liu, S. Liu, and J. Lv, *New J. Chem.* **43**, 17403–17407 (2019).
- [35] S. Shao, W. Zhu, J. Lv, Y. Wang, Y. Chen, and Y. Ma, *npj Comput. Mater.* **6**, 1–6 (2020).
- [36] Y. Sun, F. Zhang, Z. Ye, Y. Zhang, X. Fang, Z. Ding, C.-Z. Wang, M. I. Mendelev, R. T. Ott, M. J. Kramer, et al., *Sci. Rep.* **6**, 1–8 (2016).